

MIT Open Access Articles

Search for production of an $\Upsilon(1S)$ meson in association with a W or Z boson using the full 1.96 TeV $p[\bar{p}]$ collision data set at CDF

The MIT Faculty has made this article openly available. **Please share** how this access benefits you. Your story matters.

Citation: Aaltonen, T. et al. "Search for Production of an $\Upsilon(1S)$ Meson in Association with a W or Z Boson using the Full 1.96 TeV $p[\bar{p}]$ Collision Data Set at CDF." *Physical Review D* 91.5 (2015). © 2015 American Physical Society

As Published: <http://dx.doi.org/10.1103/PhysRevD.91.052011>

Publisher: American Physical Society

Persistent URL: <http://hdl.handle.net/1721.1/96145>

Version: Final published version: final published article, as it appeared in a journal, conference proceedings, or other formally published context

Terms of Use: Article is made available in accordance with the publisher's policy and may be subject to US copyright law. Please refer to the publisher's site for terms of use.



Search for production of an $\Upsilon(1S)$ meson in association with a W or Z boson using the full 1.96 TeV $p\bar{p}$ collision data set at CDF

T. Aaltonen,²¹ S. Amerio,^{39a,39b} D. Amidei,³¹ A. Anastassov,^{15,w} A. Annovi,¹⁷ J. Antos,¹² G. Apollinari,¹⁵ J. A. Appel,¹⁵ T. Arisawa,⁵² A. Artikov,¹³ J. Asaadi,⁴⁷ W. Ashmanskas,¹⁵ B. Auerbach,² A. Aurisano,⁴⁷ F. Azfar,³⁸ W. Badgett,¹⁵ T. Bae,²⁵ A. Barbaro-Galtieri,²⁶ V. E. Barnes,⁴³ B. A. Barnett,²³ P. Barria,^{41a,41c} P. Bartos,¹² M. Bauce,^{39a,39b} F. Bedeschi,^{41a} S. Behari,¹⁵ G. Bellettini,^{41a,41b} J. Bellinger,⁵⁴ D. Benjamin,¹⁴ A. Beretvas,¹⁵ A. Bhatti,⁴⁵ K. R. Bland,⁵ B. Blumenfeld,²³ A. Bocci,¹⁴ A. Bodek,⁴⁴ D. Bortoletto,³ J. Boudreau,⁴² A. Boveia,¹¹ L. Brigliadori,^{6a,6b} C. Bromberg,³² E. Brucken,²¹ J. Budagov,¹³ H. S. Budd,⁴⁴ K. Burkett,¹⁵ G. Busetto,^{39a,39b} P. Bussey,¹⁹ P. Butti,^{41a,41b} A. Buzatu,¹⁹ A. Calamba,¹⁰ S. Camarda,⁴ M. Campanelli,²⁸ F. Canelli,^{11,dd} B. Carls,²² D. Carlsmith,^{41a,41b} R. Carosi,^{41a} S. Carrillo,^{16,1} B. Casal,^{9,j} M. Casarsa,^{48a} A. Castro,^{6a,6b} P. Catastini,²⁰ D. Cauz,^{48a,48b,48c} V. Cavaliere,²² A. Cerri,^{26,e} L. Cerrito,^{28,r} Y. C. Chen,¹ M. Chertok,⁷ G. Chiarelli,^{41a} G. Chlachidze,¹⁵ K. Cho,²⁵ D. Chokheli,¹³ A. Clark,¹⁸ C. Clarke,⁵³ M. E. Convery,¹⁵ J. Conway,⁷ M. Corbo,^{15,z} M. Cordelli,¹⁷ C. A. Cox,⁷ D. J. Cox,⁷ M. Cremonesi,^{41a} D. Cruz,⁴⁷ J. Cuevas,^{9,y} R. Culbertson,¹⁵ N. d'Ascenzo,^{15,v} M. Datta,^{15,gg} P. de Barbaro,⁴⁴ L. Demortier,⁴⁵ M. Deninno,^{6a} M. D'Errico,^{39a,39b} F. Devoto,²¹ A. Di Canto,^{41a,41b} B. Di Ruzza,^{15,p} J. R. Dittmann,⁵ S. Donati,^{41a,41b} M. D'Onofrio,²⁷ M. Dorigo,^{48a,48d} A. Driutti,^{48a,48b,48c} K. Ebina,⁵² R. Edgar,³¹ A. Elagin,⁴⁷ R. Erbacher,⁷ S. Errede,²² B. Esham,²² S. Farrington,³⁸ J. P. Fernández Ramos,²⁹ R. Field,¹⁶ G. Flanagan,^{15,t} R. Forrest,⁷ M. Franklin,²⁰ J. C. Freeman,¹⁵ H. Frisch,¹¹ Y. Funakoshi,⁵² C. Galloni,^{41a,41b} A. F. Garfinkel,⁴³ P. Garosi,^{41a,41c} H. Gerberich,²² E. Gerchtein,¹⁵ S. Giagu,^{46a} V. Giakoumopoulou,³ K. Gibson,⁴² C. M. Ginsburg,¹⁵ N. Giokaris,³ P. Giromini,¹⁷ V. Glagolev,¹³ D. Glenzinski,¹⁵ M. Gold,³⁴ D. Goldin,⁴⁷ A. Golossanov,¹⁵ G. Gomez,⁹ G. Gomez-Ceballos,³⁰ M. Goncharov,³⁰ O. González López,²⁹ I. Gorelov,³⁴ A. T. Goshaw,¹⁴ K. Goulios,⁴⁵ E. Gramellini,^{6a} C. Grosso-Pilcher,¹¹ R. C. Group,^{51,15} J. Guimaraes da Costa,²⁰ S. R. Hahn,¹⁵ J. Y. Han,⁴⁴ F. Happacher,¹⁷ K. Hara,⁴⁹ M. Hare,⁵⁰ R. F. Harr,⁵³ T. Harrington-Taber,^{15,m} K. Hatakeyama,⁵ C. Hays,³⁸ J. Heinrich,⁴⁰ M. Herndon,⁵⁴ A. Hocker,¹⁵ Z. Hong,⁴⁷ W. Hopkins,^{15,f} S. Hou,¹ R. E. Hughes,³⁵ U. Husemann,⁵⁵ M. Hussein,^{32,bb} J. Huston,³² G. Introzzi,^{41a,41e,41f} M. Iori,^{46a,46b} A. Ivanov,^{7,o} E. James,¹⁵ D. Jang,¹⁰ B. Jayatilaka,¹⁵ E. J. Jeon,²⁵ S. Jindariani,¹⁵ M. Jones,⁴³ K. K. Joo,²⁵ S. Y. Jun,¹⁰ T. R. Junk,¹⁵ M. Kambeitz,²⁴ T. Kamon,^{25,47} P. E. Karchin,⁵³ A. Kasmi,⁵ Y. Kato,^{37,n} W. Ketchum,^{11,hh} J. Keung,⁴⁰ B. Kilminster,^{15,dd} D. H. Kim,²⁵ H. S. Kim,²⁵ J. E. Kim,²⁵ M. J. Kim,¹⁷ S. H. Kim,⁴⁹ S. B. Kim,²⁵ Y. J. Kim,²⁵ Y. K. Kim,¹¹ N. Kimura,⁵² M. Kirby,¹⁵ K. Knoepfel,¹⁵ K. Kondo,^{52,*} D. J. Kong,²⁵ J. Konigsberg,¹⁶ A. V. Kotwal,¹⁴ M. Kreps,²⁴ J. Kroll,⁴⁰ M. Kruse,¹⁴ T. Kuhr,²⁴ M. Kurata,⁴⁹ A. T. Laasanen,⁴³ S. Lammel,¹⁵ M. Lancaster,²⁸ K. Lannon,^{35,x} G. Latino,^{41a,41c} H. S. Lee,²⁵ J. S. Lee,²⁵ S. Leo,^{41a} S. Leone,^{41a} J. D. Lewis,¹⁵ A. Limosani,^{14,s} E. Lipeles,⁴⁰ A. Lister,^{18,a} H. Liu,⁵¹ Q. Liu,⁴³ T. Liu,¹⁵ S. Lockwitz,⁵⁵ A. Loginov,⁵⁵ D. Lucchesi,^{39a,39b} A. Lucà,¹⁷ J. Lueck,²⁴ P. Lujan,²⁶ P. Lukens,¹⁵ G. Lungu,²⁶ J. Lys,²⁶ R. Lysak,^{12,d} R. Madrak,¹⁵ P. Maestro,^{41a,41c} S. Malik,⁴⁵ G. Manca,^{27,b} A. Manousakis-Katsikakis,³ L. Marchese,^{6a,ii} F. Margaroli,^{46a} P. Marino,^{41a,41d} K. Matera,²² M. E. Mattson,⁵³ A. Mazzacone,¹⁵ P. Mazzanti,^{6a} R. McNulty,^{27,i} A. Mehta,²⁷ P. Mehtala,²¹ C. Mesropian,⁴⁵ T. Miaou,¹⁵ D. Mietlicki,³¹ A. Mitra,¹ H. Miyake,⁴⁹ S. Moed,¹⁵ N. Moggi,^{6a} C. S. Moon,^{15,z} R. Moore,^{15,ee,ff} M. J. Morello,^{41a,41d} A. Mukherjee,¹⁵ Th. Muller,²⁴ P. Murat,¹⁵ M. Mussini,^{6a,6b} J. Nachtman,^{15,m} Y. Nagai,⁴⁹ J. Naganoma,⁵² I. Nakano,³⁶ A. Napier,⁵⁰ J. Nett,⁴⁷ C. Neu,⁵¹ T. Nigmanov,⁴² L. Nodulman,² S. Y. Noh,²⁵ O. Norriella,²² L. Oakes,³⁸ S. H. Oh,¹⁴ Y. D. Oh,²⁵ I. Oksuzian,⁵¹ T. Okusawa,³⁷ R. Orava,²¹ L. Ortolan,⁴ C. Pagliarone,^{48a} E. Palencia,^{9,e} P. Palni,³⁴ V. Papadimitriou,¹⁵ W. Parker,⁵⁴ G. Pauletta,^{48a,48b,48c} M. Paulini,¹⁰ C. Paus,³⁰ T. J. Phillips,¹⁴ G. Piacentino,^{15,q} E. Pianori,⁴⁰ J. Pilot,⁷ K. Pitts,²² C. Plager,⁸ L. Pondrom,⁵⁴ S. Poprocki,^{15,f} K. Potamianos,²⁶ A. Pranko,²⁶ F. Prokoshin,^{13,aa} F. Ptohos,^{17,g} G. Punzi,^{41a,41b} I. Redondo Fernández,²⁹ P. Renton,³⁸ M. Rescigno,^{46a} F. Rimondi,^{6a,*} L. Ristori,^{41a,15} A. Robson,¹⁹ T. Rodriguez,⁴⁰ S. Rolli,^{50,h} M. Ronzani,^{41a,41b} R. Roser,¹⁵ J. L. Rosner,¹¹ F. Ruffini,^{41a,41c} A. Ruiz,⁹ J. Russ,¹⁰ V. Rusu,¹⁵ W. K. Sakumoto,⁴⁴ Y. Sakurai,⁵² L. Santi,^{48a,48c} K. Sato,⁴⁹ V. Saveliev,^{15,v} A. Savoy-Navarro,^{15,z} P. Schlabach,¹⁵ E. E. Schmidt,¹⁵ T. Schwarz,³¹ L. Scodellaro,⁹ F. Scuri,^{41a} S. Seidel,³⁴ Y. Seiya,³⁷ A. Semenov,¹³ F. Sforza,^{41a,41b} S. Z. Shalhout,⁷ T. Shears,²⁷ P. F. Shepard,⁴² M. Shimojima,^{49,u} M. Shochet,¹¹ I. Shreyber-Tecker,³³ A. Simonenko,¹³ K. Sliwa,⁵⁰ J. R. Smith,⁷ F. D. Snider,¹⁵ H. Song,⁴² V. Sorin,⁴ R. St. Denis,^{19,*} M. Stancari,¹⁵ D. Stentz,^{15,w} J. Strologas,³⁴ Y. Sudo,⁴⁹ A. Sukhanov,¹⁵ I. Suslov,¹³ K. Takemasa,⁴⁹ Y. Takeuchi,⁴⁹ J. Tang,¹¹ M. Tecchio,³¹ P. K. Teng,¹ J. Thom,^{15,f} E. Thomson,⁴⁰ V. Thukral,⁴⁷ D. Toback,⁴⁷ S. Tokar,¹² K. Tollefson,³² T. Tomura,⁴⁹ D. Tonelli,^{15,e} S. Torre,¹⁷ D. Torretta,¹⁵ P. Totaro,^{39a} M. Trovato,^{41a,41d} F. Ukegawa,⁴⁹ S. Uozumi,²⁵ G. Velev,¹⁵ C. Vellidis,¹⁵ C. Vernieri,^{41a,41d} M. Vidal,⁴³ R. Vilar,⁹ J. Vizán,^{9,cc} M. Vogel,³⁴ G. Volpi,¹⁷ F. Vázquez,^{16,l} P. Wagner,⁴⁰ R. Wallny,^{15,j} S. M. Wang,¹ D. Waters,²⁸ W. C. Wester III,¹⁵ D. Whiteson,^{40,c} A. B. Wicklund,² S. Wilbur,⁷ H. H. Williams,⁴⁰ J. S. Wilson,³¹ P. Wilson,¹⁵ B. L. Winer,³⁵ P. Wittich,^{15,f} S. Wolbers,¹⁵ H. Wolfe,³⁵ T. Wright,³¹ X. Wu,¹⁸ Z. Wu,⁵ K. Yamamoto,³⁷ D. Yamato,³⁷ T. Yang,¹⁵ U. K. Yang,²⁵ Y. C. Yang,²⁵ W.-M. Yao,²⁶ G. P. Yeh,¹⁵ K. Yi,^{15,m} J. Yoh,¹⁵ K. Yorita,⁵² T. Yoshida,^{37,k} G. B. Yu,¹⁴ I. Yu,²⁵ A. M. Zanetti,^{48a} Y. Zeng,¹⁴ C. Zhou,¹⁴ and S. Zucchelli^{6a,6b}

(CDF Collaboration)

- ¹*Institute of Physics, Academia Sinica, Taipei, Taiwan 11529, Republic of China*
²*Argonne National Laboratory, Argonne, Illinois 60439, USA*
³*University of Athens, 157 71 Athens, Greece*
⁴*Institut de Fisica d'Altes Energies, ICREA, Universitat Autònoma de Barcelona, E-08193 Bellaterra (Barcelona), Spain*
⁵*Baylor University, Waco, Texas 76798, USA*
^{6a}*Istituto Nazionale di Fisica Nucleare Bologna, I-40127 Bologna, Italy*
^{6b}*University of Bologna, I-40127 Bologna, Italy*
⁷*University of California, Davis, Davis, California 95616, USA*
⁸*University of California, Los Angeles, Los Angeles, California 90024, USA*
⁹*Instituto de Fisica de Cantabria, CSIC-University of Cantabria, 39005 Santander, Spain*
¹⁰*Carnegie Mellon University, Pittsburgh, Pennsylvania 15213, USA*
¹¹*Enrico Fermi Institute, University of Chicago, Chicago, Illinois 60637, USA*
¹²*Comenius University, 842 48 Bratislava, Slovakia; Institute of Experimental Physics, 040 01 Kosice, Slovakia*
¹³*Joint Institute for Nuclear Research, RU-141980 Dubna, Russia*
¹⁴*Duke University, Durham, North Carolina 27708, USA*
¹⁵*Fermi National Accelerator Laboratory, Batavia, Illinois 60510, USA*
¹⁶*University of Florida, Gainesville, Florida 32611, USA*
¹⁷*Laboratori Nazionali di Frascati, Istituto Nazionale di Fisica Nucleare, I-00044 Frascati, Italy*
¹⁸*University of Geneva, CH-1211 Geneva 4, Switzerland*
¹⁹*Glasgow University, Glasgow G12 8QQ, United Kingdom*
²⁰*Harvard University, Cambridge, Massachusetts 02138, USA*
²¹*Division of High Energy Physics, Department of Physics, University of Helsinki, FIN-00014 Helsinki, Finland;*
Helsinki Institute of Physics, FIN-00014 Helsinki, Finland
²²*University of Illinois, Urbana, Illinois 61801, USA*
²³*The Johns Hopkins University, Baltimore, Maryland 21218, USA*
²⁴*Institut für Experimentelle Kernphysik, Karlsruhe Institute of Technology, D-76131 Karlsruhe, Germany*
²⁵*Center for High Energy Physics: Kyungpook National University, Daegu 702-701, Korea;*
Seoul National University, Seoul 151-742, Korea; Sungkyunkwan University, Suwon 440-746, Korea;
Korea Institute of Science and Technology Information, Daejeon 305-806, Korea;
Chonnam National University, Gwangju 500-757, Korea;
Chonbuk National University, Jeonju 561-756, Korea; Ewha Womans University, Seoul 120-750, Korea
²⁶*Ernest Orlando Lawrence Berkeley National Laboratory, Berkeley, California 94720, USA*
²⁷*University of Liverpool, Liverpool L69 7ZE, United Kingdom*
²⁸*University College London, London WC1E 6BT, United Kingdom*
²⁹*Centro de Investigaciones Energeticas Medioambientales y Tecnológicas, E-28040 Madrid, Spain*
³⁰*Massachusetts Institute of Technology, Cambridge, Massachusetts 02139, USA*
³¹*University of Michigan, Ann Arbor, Michigan 48109, USA*
³²*Michigan State University, East Lansing, Michigan 48824, USA*
³³*Institution for Theoretical and Experimental Physics, ITEP, Moscow 117259, Russia*
³⁴*University of New Mexico, Albuquerque, New Mexico 87131, USA*
³⁵*The Ohio State University, Columbus, Ohio 43210, USA*
³⁶*Okayama University, Okayama 700-8530, Japan*
³⁷*Osaka City University, Osaka 558-8585, Japan*
³⁸*University of Oxford, Oxford OX1 3RH, United Kingdom*
^{39a}*Istituto Nazionale di Fisica Nucleare, Sezione di Padova, I-35131 Padova, Italy*
^{39b}*University of Padova, I-35131 Padova, Italy*
⁴⁰*University of Pennsylvania, Philadelphia, Pennsylvania 19104, USA*
^{41a}*Istituto Nazionale di Fisica Nucleare Pisa, I-56127 Pisa, Italy*
^{41b}*University of Pisa, I-56127 Pisa, Italy*
^{41c}*University of Siena, I-56127 Pisa, Italy*
^{41d}*Scuola Normale Superiore, I-56127 Pisa, Italy*
^{41e}*INFN Pavia, I-27100 Pavia, Italy*
^{41f}*University of Pavia, I-27100 Pavia, Italy*
⁴²*University of Pittsburgh, Pittsburgh, Pennsylvania 15260, USA*
⁴³*Purdue University, West Lafayette, Indiana 47907, USA*
⁴⁴*University of Rochester, Rochester, New York 14627, USA*
⁴⁵*The Rockefeller University, New York, New York 10065, USA*

- ^{46a}*Istituto Nazionale di Fisica Nucleare, Sezione di Roma 1, I-00185 Roma, Italy*
^{46b}*Sapienza Università di Roma, I-00185 Roma, Italy*
⁴⁷*Mitchell Institute for Fundamental Physics and Astronomy, Texas A&M University, College Station, Texas 77843, USA*
^{48a}*Istituto Nazionale di Fisica Nucleare Trieste, I-33100 Udine, Italy*
^{48b}*Gruppo Collegato di Udine, I-33100 Udine, Italy*
^{48c}*University of Udine, I-33100 Udine, Italy*
^{48d}*University of Trieste, I-34127 Trieste, Italy*
⁴⁹*University of Tsukuba, Tsukuba, Ibaraki 305, Japan*
⁵⁰*Tufts University, Medford, Massachusetts 02155, USA*
⁵¹*University of Virginia, Charlottesville, Virginia 22906, USA*
⁵²*Waseda University, Tokyo 169, Japan*
⁵³*Wayne State University, Detroit, Michigan 48201, USA*
⁵⁴*University of Wisconsin, Madison, Wisconsin 53706, USA*
⁵⁵*Yale University, New Haven, Connecticut 06520, USA*
(Received 17 December 2014; published 17 March 2015)

Production of the $\Upsilon(1S)$ meson in association with a vector boson is a rare process in the standard model with a cross section predicted to be below the sensitivity of the Tevatron. Observation of this process could signify contributions not described by the standard model or reveal limitations with the current nonrelativistic quantum-chromodynamic models used to calculate the cross section. We perform a search for this process using the full Run II data set collected by the CDF II detector corresponding to an integrated luminosity of 9.4 fb^{-1} . The search considers the $\Upsilon \rightarrow \mu\mu$ decay and the decay of the W and Z bosons into muons and electrons. In these purely leptonic decay channels, we observe one YW candidate with an expected background of 1.2 ± 0.5 events, and one YZ candidate with an expected background of 0.1 ± 0.1 events. Both observations are consistent with the predicted background

*Deceased.

^aVisitor from University of British Columbia, Vancouver, BC V6T 1Z1, Canada.

^bVisitor from Istituto Nazionale di Fisica Nucleare, Sezione di Cagliari, 09042 Monserrato (Cagliari), Italy.

^cVisitor from University of California Irvine, Irvine, California 92697, USA.

^dVisitor from Institute of Physics, Academy of Sciences of the Czech Republic, 182 21, Czech Republic.

^eVisitor from CERN, CH-1211 Geneva, Switzerland.

^fVisitor from Cornell University, Ithaca, New York 14853, USA.

^gVisitor from University of Cyprus, Nicosia CY-1678, Cyprus.

^hVisitor from Office of Science, U.S. Department of Energy, Washington, DC 20585, USA.

ⁱVisitor from University College Dublin, Dublin 4, Ireland.

^jVisitor from ETH, 8092 Zürich, Switzerland.

^kVisitor from University of Fukui, Fukui City, Fukui Prefecture 910-0017, Japan.

^lVisitor from Universidad Iberoamericana, Lomas de Santa Fe, México, C.P. 01219, Distrito Federal.

^mVisitor from University of Iowa, Iowa City, Iowa 52242, USA.

ⁿVisitor from Kinki University, Higashi-Osaka City 577-8502, Japan.

^oVisitor from Kansas State University, Manhattan, Kansas 66506, USA.

^pVisitor from Brookhaven National Laboratory, Upton, New York 11973, USA.

^qVisitor from Istituto Nazionale di Fisica Nucleare, Sezione di Lecce, Via Arnesano, I-73100 Lecce, Italy.

^rVisitor from Queen Mary, University of London, London E1 4NS, United Kingdom.

^sVisitor from University of Sydney, NSW 2006, Australia.

^tVisitor from Muons, Inc., Batavia, Illinois 60510, USA.

^uVisitor from Nagasaki Institute of Applied Science, Nagasaki 851-0193, Japan.

^vVisitor from National Research Nuclear University, Moscow 115409, Russia.

^wVisitor from Northwestern University, Evanston, Illinois 60208, USA.

^xVisitor from University of Notre Dame, Notre Dame, Indiana 46556, USA.

^yVisitor from Universidad de Oviedo, E-33007 Oviedo, Spain.

^zVisitor from CNRS-IN2P3, Paris F-75205, France.

^{aa}Visitor from Universidad Tecnica Federico Santa Maria, 110v Valparaiso, Chile.

^{bb}Visitor from The University of Jordan, Amman 11942, Jordan.

^{cc}Visitor from Universite catholique de Louvain, 1348 Louvain-La-Neuve, Belgium.

^{dd}Visitor from University of Zürich, 8006 Zürich, Switzerland.

^{ee}Visitor from Massachusetts General Hospital, Boston, Massachusetts 02114, USA.

^{ff}Visitor from Harvard Medical School, Boston, Massachusetts 02114, USA.

^{gg}Visitor from Hampton University, Hampton, Virginia 23668, USA.

^{hh}Visitor from Los Alamos National Laboratory, Los Alamos, New Mexico 87544, USA.

ⁱⁱVisitor from Università degli Studi di Napoli Federico I, I-80138 Napoli, Italy.

contributions. The resulting upper limits on the cross section for $\Upsilon + W/Z$ production are the most sensitive reported from a single experiment and place restrictions on potential contributions from non-standard-model physics.

DOI: [10.1103/PhysRevD.91.052011](https://doi.org/10.1103/PhysRevD.91.052011)

PACS numbers: 14.70.-e, 12.39.Jh, 14.40.Pq

I. INTRODUCTION

The standard model production of an upsilon (Υ) meson in association with a W boson or a Z boson is a rare process whose rate was first calculated in Ref. [1], where ΥW and ΥZ production occur through the parton-level processes producing $W + b\bar{b}$ and $Z + b\bar{b}$ final states, in which the $b\bar{b}$ pair may form a bound state (either an Υ or an excited bottomonium state that decays to an Υ). More recently, rates for these processes have been calculated at next-to-leading order in the strong-interaction coupling for proton-antiproton ($p\bar{p}$) collisions at 1.96 TeV center-of-mass energy and proton-proton collisions at 8 and 14 TeV [2].

The cross sections calculated for ΥW and ΥZ production in $p\bar{p}$ collisions at 1.96 TeV are 43 fb and 34 fb, respectively. These values were calculated at leading order using the MADONIA quarkonium generator [3] as detailed below and are roughly a factor of 10 smaller than the earlier calculations from Ref. [1]. The calculations of these processes are very sensitive to nonrelativistic quantum-chromodynamic (NRQCD) models, especially the numerical values of the long-distance matrix elements (LDME), which determine the probability that a $b\bar{b}$ will form a bottomonium state. Measurements of $\Upsilon + W/Z$ cross sections are important for validating these NRQCD models.

Supersymmetry (SUSY) is an extension of the standard model (SM) which has not been observed. Reference [1] describes some SUSY models in which charged Higgs bosons can decay into ΥW final states with a large branching fraction (\mathcal{B}). Similarly, in addition to the expected decays of a SM Higgs to an ΥZ pair, further light neutral scalars may decay into ΥZ . Therefore, if the observed rate of ΥW and/or ΥZ production is significantly larger than the predicted SM rate, it may be an indication of physics not described by the SM.

In 2003, the CDF collaboration reported [4] a search for the associated production of an Υ meson and a W or Z boson. In that analysis, a sample corresponding to 83 pb⁻¹ of 1.8 TeV $p\bar{p}$ collision data collected with the Run I CDF detector was used to set upper limits on the production cross sections (σ) at the 95% confidence level (C.L.) of $\sigma(p\bar{p} \rightarrow \Upsilon W) \times \mathcal{B}(\Upsilon \rightarrow \mu^+\mu^-) < 2.3$ pb and $\sigma(p\bar{p} \rightarrow \Upsilon Z) \times \mathcal{B}(\Upsilon \rightarrow \mu^+\mu^-) < 2.5$ pb. The ATLAS collaboration has also reported on the related channels of $J/\psi + W/Z$ production [5,6].

Here we present a search for $\Upsilon + W/Z$ production, using a sample corresponding to 9.4 fb⁻¹ of 1.96 TeV $p\bar{p}$ collision data collected with the CDF II detector. We use the dimuon decay channel to identify the Υ meson. We use

only the electron and muon decay channels of the W and Z bosons, which give the best sensitivities for this search.

II. THE CDF DETECTOR

The CDF II detector is a nearly azimuthally and forward-backward symmetric detector designed to study $p\bar{p}$ collisions at the Tevatron. It is described in detail in Ref. [7]. It consists of a magnetic spectrometer surrounded by calorimeters and a muon-detection system. Particle trajectories are expressed in a cylindrical coordinate system, with the z axis along the proton beam and the x axis pointing outward from the center of the Tevatron. The azimuthal angle (ϕ) is defined with respect to the x direction. The polar angle (θ) is measured with respect to the z direction, and the pseudorapidity (η) is defined as $\eta = -\ln(\tan\frac{\theta}{2})$. The momentum of charged particles is measured by the tracking system, consisting of silicon strip detectors surrounded by an open-cell drift chamber, all immersed in a 1.4 T solenoidal magnetic field. The tracking system provides charged-particle trajectory (track) information with good efficiency in the range $|\eta| \lesssim 1.0$. The tracking system is surrounded by pointing-geometry tower calorimeters, that measure the energies of electrons, photons, and jets of hadronic particles. The electromagnetic calorimeters consist of scintillating tile and lead absorber, while the hadronic calorimeters are composed of scintillating tiles with steel absorber. The calorimeter system includes central and plug subdetectors, with the central region covering $|\eta| < 1.1$ and the plug region covering the range $1.1 < |\eta| < 3.6$. The muon system is composed of planar multiwire drift chambers. In the central region, four layers of chambers located just outside the calorimeter cover the region $|\eta| < 0.6$. An additional 60 cm of iron shielding surrounds this system, and behind that is a second subdetector composed of another four layers of chambers. A third muon subdetector covers the region $0.6 < |\eta| < 1.0$, and a fourth subdetector extends coverage to $|\eta| < 1.5$. Cherenkov luminosity counters measure the rate of inelastic collisions, that is converted into the instantaneous luminosity. A three-level online event-selection system (trigger) is used to reduce the event rate from 2.5 MHz to approximately 100 Hz. The first level consists of specialized hardware, while the second is a mixture of hardware and fast software algorithms. The software-based third-level trigger has access to a similar set of information to that available in the off-line reconstruction.

III. MONTE CARLO AND DATA SAMPLES

We use a number of quantities based on track and calorimeter information in the event selection. The transverse momentum of a charged particle is $p_T = p \sin \theta$, where p is the particle's momentum. The analogous quantity measured with the calorimeter is transverse energy, $E_T = E \sin \theta$. The missing transverse energy, \vec{E}_T is defined as $\vec{E}_T = -\sum_i E_T^i \hat{n}_i$, where \hat{n}_i is a unit vector perpendicular to the beam axis and pointing to the center of the i th calorimeter tower. The \vec{E}_T is adjusted for high-energy muons, which deposit only a small fraction of their energies in the calorimeter, and off-line corrections applied to the measured energies of reconstructed jets [8] which result from the hadronization of quarks and gluons. We define $E_T = |\vec{E}_T|$. The invariant mass of two leptons is $M_{\ell\ell} = \sqrt{(E_{\ell 1} + E_{\ell 2})^2/c^4 - |\vec{p}_{\ell 1} + \vec{p}_{\ell 2}|^2/c^2}$, and the transverse mass of a lepton and neutrino (estimated with \vec{E}_T) is $M_T = \sqrt{2E_T^\ell \vec{E}_T (1 - \cos \xi)}/c^3$ where ξ is the angle between the lepton track and \vec{E}_T vector in the transverse plane. For muons, p_ℓ and p_T^ℓ are used rather than their measured energies E_ℓ and E_T^ℓ in the definitions of $M_{\ell\ell}$ and M_T .

The analysis uses events selected with triggers requiring a high- E_T central electron candidate ($E_T > 18$ GeV, $|\eta| < 1.0$) or a high- p_T central muon candidate ($p_T > 18$ GeV/ c , $|\eta| < 1.0$). The integrated luminosity of these samples is 9.4 fb^{-1} . All the search channels include the $\Upsilon \rightarrow \mu\mu$ signal, so we only use data acquired when the muon detectors were operational, resulting in the same integrated luminosity for the electron and muon samples.

We also use a low- p_T dimuon-triggered Υ sample to estimate one of the backgrounds as detailed in Sec. V. The dimuon invariant-mass distribution from this low- p_T sample, whose integrated luminosity is 7.3 fb^{-1} , is shown in Fig. 1 for the mass range in the region of the Υ resonances.

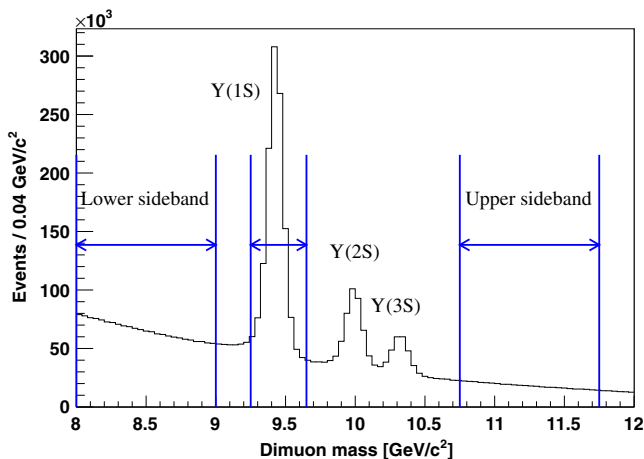


FIG. 1 (color online). Dimuon invariant-mass spectrum in CDF II data from events contained within the low- p_T dimuon-triggered sample. Shown are the defined Υ signal region and the sideband regions used for background determination.

We produce simulated event samples of the signal processes, ΥW and ΥZ , by first generating events with MADGRAPH [9] and its quarkonium extension MADONIA [3]. We include all ΥW and ΥZ processes from Ref. [1] and the LDME values relevant for the Tevatron from Ref. [10]. An explanation of how LDME values are determined from fits to quarkonia data is given in Ref. [11], although the values obtained in this reference are specific for the LHC. PYTHIA [12] is used to simulate the Υ , W , and Z decays and parton showering. Generated Υ mesons are forced to decay to two muons. We use a GEANT3-based [13] detector simulation to model the response of the CDF II detector [14].

IV. EVENT SELECTION

Events are selected with Υ mesons decaying to muon pairs and decays of vector bosons resulting in at least one electron or muon. In this analysis we have two categories of lepton candidates: low- p_T muon candidates with $1.5 < p_T < 15$ GeV/ c from the Υ decay and high- E_T (or p_T) electron (or muon) candidates from the W or Z decay.

High- E_T electron candidates are identified by matching a track to energy deposited within the calorimeter. Muon candidates are formed from charged particle tracks matched to minimum ionizing energy deposition in the calorimeter, which may or may not be matched to track segments in the muon chambers situated behind the calorimeters. Lepton reconstruction algorithms are described in detail elsewhere [15].

Electron candidates are distinguished by whether they are found in the central or forward calorimeters ($|\eta| > 1.1$) where only silicon tracking information is available. The electron selection relies on track quality, track-calorimeter matching, calorimeter energy, calorimeter profile shape, and isolation information. Most muon candidates rely on direct detection in the muon chambers, which are distinguished by their acceptance in pseudorapidity: central muon detectors ($|\eta| < 0.6$), central muon extension detectors ($0.6 < |\eta| < 1.0$), and the intermediate muon detector ($1.0 < |\eta| < 1.5$). Remaining muon candidates rely on track matches to energy deposits consistent with a minimum ionizing charged particle in the central and forward electromagnetic calorimeters respectively, and which fail to have an associated track segment in the muon subdetectors. All high- E_T (or p_T) leptons are required to be isolated by imposing the condition that the sum of the transverse energy of the calorimeter towers in a cone of $\Delta R \equiv \sqrt{(\Delta\phi)^2 + (\Delta\eta)^2} = 0.4$ around the lepton is less than 10% of the electron E_T (muon p_T).

The analysis uses the high- E_T electron triggered, and high- p_T muon triggered, data sets where events are additionally required to contain $\Upsilon(1S)$ candidates using the Υ decay to two low- p_T muons ($1.5 < p_T < 15$ GeV/ c). We define the $\Upsilon(1S)$ region as the invariant-mass range $9.25 < M_{\mu\mu} < 9.65$ GeV/ c^2 . We do not use $\Upsilon(2S)$ or

$\Upsilon(3S)$ decays. We define two sideband regions, $8.00 < M_{\mu\mu} < 9.00 \text{ GeV}/c^2$ and $10.75 < M_{\mu\mu} < 11.75 \text{ GeV}/c^2$, for obtaining background estimates. Events are required to have at least two low- p_T muon candidates whose invariant mass lies within the $\Upsilon(1S)$ region. To increase the efficiency for reconstructing Υ candidates, we use looser quality requirements on these low- p_T muon candidates than for the high- p_T muon candidates used in the vector-boson reconstruction. In particular, there are no isolation requirements on the Υ muon candidates, and geometrical matching requirements between charged particles in the tracker and track segments in the muon detectors are less stringent. Most low- p_T muon candidates surviving event selection are found to be within acceptance of the muon chambers ($|\eta| < 1.5$). In the small fraction of events (less than 2%) that have more than two low- p_T muons identified, we randomly choose one pair of those muons.

We then look for additional high-energy electron (or muon) candidates consistent with the decay of a vector boson. Events with exactly one high-energy lepton candidate, ℓ , which will henceforth refer to an electron or muon, with E_T (p_T) greater than 20 GeV (GeV/c), in addition to the $\Upsilon \rightarrow \mu^+\mu^-$ candidate, and significant missing transverse energy ($\cancel{E}_T > 20 \text{ GeV}$) are selected as $\Upsilon + (W \rightarrow \ell\nu)$ candidates. Such candidates are further required to have a transverse mass in the range $50 < M_T < 90 \text{ GeV}/c^2$, as expected from a W boson decay. Figures 2 and 3 show the distributions of these quantities as predicted from the simulated $\Upsilon + W$ event samples.

Events with two oppositely charged high-energy lepton candidates of same flavor are selected as $\Upsilon + (Z \rightarrow \ell^+\ell^-)$ candidates. The $\Upsilon + (Z \rightarrow \ell\ell)$ candidates are selected by requiring one additional high- E_T (p_T) electron (muon) candidate with E_T (p_T) $> 20 \text{ GeV}$ (GeV/c) and a second candidate with the same flavor but opposite charge and E_T (p_T) $> 15 \text{ GeV}$ (GeV/c). Both additional lepton

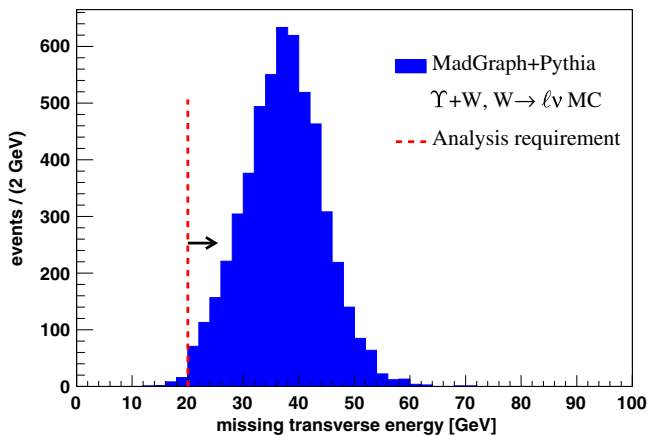


FIG. 2 (color online). Missing-transverse-energy distributions predicted for signal $\Upsilon + (W \rightarrow \ell\nu)$ events. The distributions are shown for events that satisfy all other event requirements. The scale of the vertical axis is arbitrary.

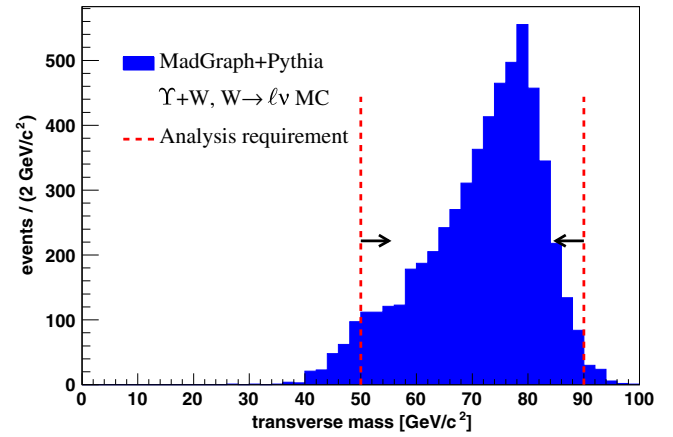


FIG. 3 (color online). Transverse-mass distributions predicted for signal $\Upsilon + (W \rightarrow \ell\nu)$ events. The distributions are shown for events that satisfy all other event requirements. The scale of the vertical axis is arbitrary.

candidates are required to be isolated and have an invariant mass in the range $76 < M_{\ell\ell} < 106 \text{ GeV}/c^2$. The invariant-mass distribution predicted from the simulated $\Upsilon + (Z \rightarrow \ell\ell)$ event samples is shown in Fig. 4.

The total signal efficiencies, after all selection criteria are applied, are determined from simulated event samples to be 1.8% for $\Upsilon + (W \rightarrow e\nu)$, 1.3% for $\Upsilon + (W \rightarrow \mu\nu)$, 1.8% for $\Upsilon + (Z \rightarrow ee)$, and 1.4% for $\Upsilon + (Z \rightarrow \mu\mu)$ events. These efficiencies do not include the branching fractions for $\Upsilon \rightarrow \mu\mu$ and the electronic and muonic decays of the vector bosons. The low acceptances are primarily driven by the geometric acceptance of the drift chamber for the two low- p_T muons from the Υ decay. We expect a small contribution to the $W \rightarrow \ell\nu$ acceptance from $W \rightarrow \tau\nu$ events where the tau lepton decays to an electron or muon. The contribution is determined to be less than 2% of the acceptance, and is therefore neglected. The contribution

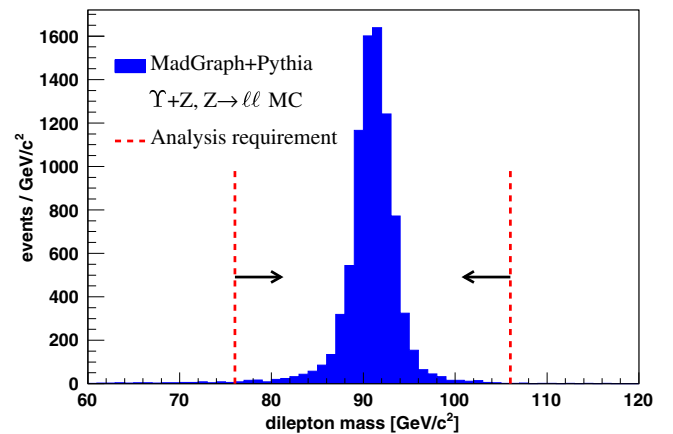


FIG. 4 (color online). Dilepton invariant-mass distribution predicted for signal $\Upsilon + (Z \rightarrow \ell\ell)$ events. The distribution is shown for events that satisfy all other event requirements. The scale of the vertical axis is arbitrary.

TABLE I. Efficiencies for the $(\Upsilon \rightarrow \mu\mu) + (W \rightarrow \ell\nu)$ selection criteria. The individual efficiencies for each requirement, in the given order, are listed with the total at the bottom. The uncertainty on the total efficiency is discussed in the text.

	$\Upsilon + (W \rightarrow e\nu)$	$\Upsilon + (W \rightarrow \mu\nu)$
$\Upsilon(1S) \rightarrow \mu\mu$ candidate	6.8%	6.8%
One additional high- $E_T(p_T)$ isolated e or μ candidate	55%	46%
High- $E_T(p_T)$ lepton candidate is triggerable	55%	52%
$\cancel{E}_T > 20$ GeV	96%	94%
$50 < M_T < 90$ GeV/ c^2	94%	95%
Trigger efficiency	97%	92%
Total	$(1.8 \pm 0.4)\%$	$(1.3 \pm 0.3)\%$

TABLE II. Efficiencies for the $(\Upsilon \rightarrow \mu\mu) + (Z \rightarrow \ell\ell)$ selection criteria. The individual efficiencies for each requirement, in the given order, are listed with the total at the bottom. The uncertainty on the total efficiency is discussed in the text. OS means opposite sign.

	$\Upsilon + (Z \rightarrow ee)$	$\Upsilon + (Z \rightarrow \mu\mu)$
$\Upsilon(1S) \rightarrow \mu\mu$ candidate	6.7%	7.0%
Two additional OS high- $E_T(p_T)$ isolated e or μ candidates	32%	25%
One of the two high- $E_T(p_T)$ lepton candidates is triggerable	86%	80%
$76 < M_{\ell\ell} < 106$ GeV/ c^2	99%	99%
Trigger efficiency	98%	95%
Total	$(1.8 \pm 0.4)\%$	$(1.4 \pm 0.3)\%$

from $Z \rightarrow \tau\tau$ events to the $Z \rightarrow \ell\ell$ channels is found to be negligible.

Summaries of the selection criteria and their associated efficiencies are given in Tables I and II.

V. BACKGROUNDS

There are two main background contributions to the samples of ΥW and ΥZ signal candidates after the final selection: events containing a correctly identified W/Z candidate and a misidentified Υ candidate (real W/Z +fake Υ) and those with a correctly identified Υ candidate and a misidentified W/Z candidate (real Υ +fake W/Z). Generic dimuon backgrounds, originating predominantly from $b\bar{b}$ production, contribute events in the $\Upsilon(1S)$ mass range and are the primary source of fake Υ candidates. Misidentification of jets as leptons can mimic the decay signatures of W and Z bosons. In the case of Z candidates, where two leptons are required, this background is negligible.

The real W/Z +fake Υ background contributions are estimated by counting the number of W or Z candidate events in the high- p_T lepton data samples that additionally contain a dimuon candidate in the sideband region of the dimuon spectrum (defined in Fig. 1). An exponential fit to these sideband regions is used to determine a ratio of the areas of the signal to sideband regions, which is then applied to these numbers for an estimate of this background contribution.

The probabilities for reconstructed jets to be misidentified as leptons are measured in jet-enriched data samples as

functions of the jet E_T and lepton type, and are corrected for the contributions of leptons from W and Z boson decays, as more fully described in Ref. [16]. To estimate real Υ +fake W/Z background contributions, we select from the low- p_T dimuon data sample events containing a high- E_T jet instead of a high- E_T (p_T) isolated lepton candidate that otherwise satisfy the full selection criteria. Background estimates are obtained using the measured probabilities associated with each of the jets within these events as weighting factors on the potential contribution of each. The low- p_T dimuon sample is relied upon to extract these background estimates because a strong correlation between high- p_T lepton trigger selection requirements and jet-to-lepton misidentification rates renders the high- p_T lepton data set unsuitable for the chosen methodology. To interpolate between the two samples, additional small corrections are applied to account for differences in the integrated luminosities of the two samples and Υ selection inefficiencies in the low- p_T dimuon sample originating from trigger requirements.

In evaluating the real Z +fake Υ background contribution, no events containing Υ candidates in the sideband mass regions are observed. Background contributions to the corresponding signal samples are therefore estimated by extrapolating from the estimated real W +fake Υ background contributions, using the ratio of Z -to- W cross sections. This makes the assumption that the probability for misidentifying a $\Upsilon(1S)$ is independent of the type of vector boson. In calculating cross-section limits, we also account for small background contributions from ΥZ

TABLE III. Systematic uncertainties associated with the signal expectation.

Luminosity	6%
Y muon identification	4%
High- $E_T(p_T)$ lepton identification	1%
High- $E_T(p_T)$ lepton trigger efficiency	1%
PDFs	12%
LDMEs	6%
Double parton scattering	15%
Event selection efficiency	3%
Total	22%

production to the ΥW samples, originating from events in which one of the two leptons produced in the Z boson decay is not reconstructed.

VI. SYSTEMATIC UNCERTAINTIES

For determining cross-section limits we incorporate systematic uncertainties on the signal expectation and the background predictions. Systematic uncertainties on the signal expectation include those associated with the integrated luminosity measurement, low- p_T muon identification, high- $E_T(p_T)$ lepton identification, high- $E_T(p_T)$ lepton trigger efficiency, theoretical modeling of the signal, and efficiencies of the event selection criteria. The upsilon-muon identification uncertainty is derived from studies that use data and simulated samples of $J/\psi \rightarrow \mu\mu$ as described in Ref. [17]. Lepton identification and trigger efficiencies are measured using samples of leptonic Z decays [16]. Requirements of $E_T > 20$ GeV ($p_T > 20$ GeV/ c) for electrons (muons) matched to lepton trigger objects ensure a uniform trigger efficiency over the lepton momentum spectra.

We use the CTEQ6L parton distribution functions (PDFs) [18] for generating the MADGRAPH samples. To estimate the acceptance uncertainty associated with the choice of PDFs, we generate additional samples using MSTW PDFs [19] and take the difference in the estimated signal acceptance as the uncertainty.

We vary the bottomonium LDMEs from Ref. [10] by one standard deviation to estimate their effect on the signal acceptance. This procedure results in an additional 6% systematic uncertainty on the signal acceptance. These uncertainties correspond only to those associated with the

procedure for computing LDMEs described within the cited reference. Allowing for a wider range of assumptions within the LDME calculations gives rise to additional uncertainties, which are not accounted for in this analysis. However, if an uncertainty of 20% were to be placed on the LDMEs, the cross-section limits we obtain would only increase by about 10%.

With respect to uncertainties associated with event selection criteria, we vary the E_T by $\pm 10\%$ (an estimate of the E_T resolution) in the simulated signal samples to quantify the effect of E_T resolution.

It is possible for the Υ meson and the W or Z boson to originate from different parton-parton interactions in the same $p\bar{p}$ collision. This double-parton-scattering process is difficult to identify, but estimates have been made for several related final states using LHC and Tevatron data (see for example Ref. [5] where J/ψ production in association with a W boson was studied by the ATLAS collaboration). These estimates, together with a calculation using the Υ and vector boson cross sections at the Tevatron collision energy lead to an estimated effect of approximately 15%. Based on lack of knowledge on double-parton scattering, we assign this effect as a systematic uncertainty on the signal acceptance. In Table III we summarize all investigated systematic uncertainties associated with the signal expectation.

Uncertainties on predicted background contributions are also incorporated into the cross-section limits. For the real W/Z + fake Υ background, we use the statistical uncertainty originating from the small sample size in the sideband regions used for making this estimate. We assign a 50% uncertainty to the real Υ + fake W/Z background based on the application of uncertainties associated with the measured jet-to-lepton misidentification rates.

VII. RESULTS

Table IV summarizes the predicted signal and background contributions, and number of observed events for each of the search samples using data from 9.4 fb^{-1} of integrated luminosity at CDF. We observe one $\Upsilon + (W \rightarrow \ell\nu)$ candidate with a total expected background of 1.2 ± 0.5 events. In the observed $\Upsilon + (W \rightarrow \ell\nu)$ candidate the electron has $p_T = 27.4$ GeV, and the two muons with an invariant mass in the $\Upsilon(1S)$ region have p_T s of 3.8 GeV/ c

TABLE IV. Summary of signal expectation (N_{sig}), background estimations (N_{bg}), and observed events (N_{obs}).

	$\Upsilon + W \rightarrow e\nu$	$\Upsilon + W \rightarrow \mu\nu$	$\Upsilon + W \rightarrow \ell\nu$	$\Upsilon + Z \rightarrow ee$	$\Upsilon + Z \rightarrow \mu\mu$	$\Upsilon + Z \rightarrow \ell\ell$
N_{sig}	0.019 ± 0.004	0.014 ± 0.003	0.034 ± 0.007	0.0048 ± 0.0011	0.0037 ± 0.0008	0.0084 ± 0.0018
N_{bg} (fake Υ)	0.7 ± 0.4	0.4 ± 0.3	1.1 ± 0.5	0.07 ± 0.07	0.04 ± 0.04	0.1 ± 0.1
N_{bg} (fake W/Z)	0.06 ± 0.04	0	0.06 ± 0.04	0	0	0
N_{bg} ($\Upsilon + Z$)	0.0006 ± 0.0001	0.0033 ± 0.0007	0.0039 ± 0.0009			
N_{bg} (total)	0.8 ± 0.4	0.4 ± 0.3	1.2 ± 0.5	0.07 ± 0.07	0.04 ± 0.04	0.1 ± 0.1
N_{obs}	0	1	1	0	1	1

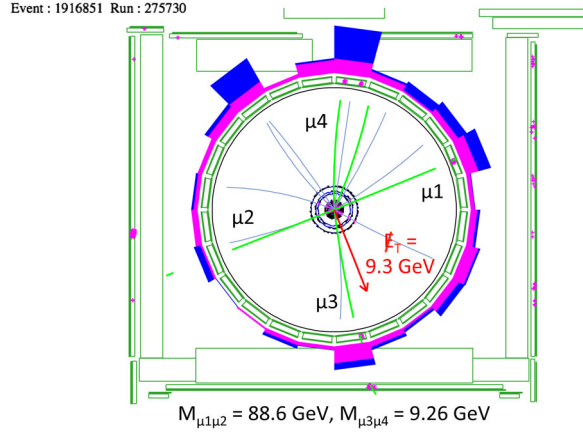


FIG. 5 (color online). Event display of the observed ΥZ candidate, showing the muon candidates identified from the Υ and Z decays. The view is in the transverse (r - ϕ) plane of the detector, where the inner core is the silicon vertex tracker, and the larger circle is the outer radius of the drift chamber where the tracks of charged particle with $p_T > 1.5$ GeV/ c are shown. The height of the surrounding pink and blue “towers” is roughly proportional to the energy deposits in the electromagnetic and hadronic compartments of the calorimeter, from which the E_T magnitude and direction (red arrow) is computed. Measurement hits in the muon chambers are shown in the outermost box-shaped structure.

and 7.1 GeV/ c . The E_T in this event is 30.8 GeV, which, with the electron gives a transverse mass of 58.1 GeV/ c^2 .

We also observe one $\Upsilon + (Z \rightarrow \ell\ell)$ candidate with a total expected background of 0.1 ± 0.1 events. An event display of the $\Upsilon + (Z \rightarrow \ell\ell)$ candidate is shown in Fig. 5. This is the first observed $\Upsilon + (Z \rightarrow \ell\ell)$ candidate event at the Tevatron. The two high- p_T muon candidates have an invariant mass of 88.6 GeV/ c^2 , and the two low- p_T muon candidates have an invariant mass of 9.26 GeV/ c^2 . All muon candidates are detected in the central region of the detector. The invariant mass of all four muon candidates is 98.4 GeV/ c^2 . Further properties of the muons in this event are given in Table VI.

Having observed no clear evidence for a $\Upsilon + W/Z$ signal, we set 90% C.L. and 95% C.L. upper limits on the ΥW and ΥZ production cross sections. We use the branching fractions of $\Upsilon \rightarrow \mu\mu$ (0.0248), $W \rightarrow \ell\nu$ (0.107), and $Z \rightarrow \ell\ell$ (0.0336) from Ref. [20]. A Bayesian

TABLE V. Cross-section upper limits for ΥW and ΥZ production. This analysis utilizes 9.4 fb^{-1} of CDF Run II data. The CDF Run I analysis utilized 83 pb^{-1} of CDF Run I data.

	ΥW	ΥZ
90% C.L. expected limit (pb)	4.4	9.9
90% C.L. observed limit (pb)	4.4	16
95% C.L. expected limit (pb)	5.6	13
95% C.L. observed limit (pb)	5.6	21
Run I 95% C.L. observed limit (pb)	93	101

TABLE VI. Kinematic properties of the muons in the observed $\Upsilon + Z$ candidate displayed in Fig. 5. Isolation is defined as the sum of calorimeter energy in a cone of $\Delta R = 0.4$ around the muon candidate as a fraction of the muon momentum. The longitudinal position z_0 (along the beam line) of each muon candidate suggests all muons come from the same primary $p\bar{p}$ interaction vertex.

	Muon 1	Muon 2	Muon 3	Muon 4
p_x (GeV/ c)	-34.6	34.8	0.823	-0.106
p_y (GeV/ c)	-14.0	13.8	-6.25	3.29
p_z (GeV/ c)	-39.2	10.6	-2.20	-2.56
E (GeV)	54.2	39.0	6.68	4.17
p_T (GeV/ c)	37.4	37.5	6.3	3.3
η	-0.92	0.28	-0.34	-0.72
ϕ (rads)	-2.76	0.38	-1.44	1.60
Isolation	0.03	0.00	0.64	0.35
z_0 (cm)	41.2	41.1	41.0	41.3

technique is employed, described in Ref. [21], where the posterior probability density was constructed from the joint Poisson probability of observing the data in each vector boson decay channel, integrating over the uncertainties of the normalization parameters using Gaussian prior-probability densities. A non-negative constant prior in the signal rate was assumed. The expected and observed limits are shown in Table V and compared to the observed limits from the CDF Run I analysis [4].

VIII. CONCLUSIONS

We search for $\Upsilon + W/Z$ production using the leptonic decay channels of the vector bosons and dimuon decay channel of the Υ . The search utilizes the full CDF Run II data set. Having observed no significant excess of events with respect to standard model predictions, we set 95% C.L. upper limits on the $\Upsilon + W/Z$ cross sections. The limits are $\sigma(p\bar{p} \rightarrow \Upsilon W) < 5.6$ pb and $\sigma(p\bar{p} \rightarrow \Upsilon Z) < 21$ pb which are the most stringent bounds on these processes to date. Under the assumption that potential non-SM physics contributions to the $\Upsilon + W/Z$ final state do not significantly impact the kinematic properties of events, these limits can be interpreted as cross section (times branching ratio to $\Upsilon + W/Z$) limits on non-SM physics processes contributing to this final state. Potential non-standard-model heavy particles decaying to $\Upsilon + W/Z$ final states are likely to result in leptons that are more central than those from standard-model $\Upsilon + W/Z$ production and therefore provide higher signal acceptance. Hence, the limits presented here can be considered as conservative limits on such processes.

ACKNOWLEDGMENTS

We would like to acknowledge K. W. Lai for suggesting the search for these processes, and thank P. Artoisenet and

J.-P. Lansberg for many useful discussions and help with theoretical inputs into the MADGRAPH simulation. We thank the Fermilab staff and the technical staffs of the participating institutions for their vital contributions. This work was supported by the U.S. Department of Energy and National Science Foundation; the Italian Istituto Nazionale di Fisica Nucleare; the Ministry of Education, Culture, Sports, Science and Technology of Japan; the Natural Sciences and Engineering Research Council of Canada; the National Science Council of the Republic of China; the Swiss National Science

Foundation; the A. P. Sloan Foundation; the Bundesministerium für Bildung und Forschung, Germany; the Korean World Class University Program, the National Research Foundation of Korea; the Science and Technology Facilities Council and the Royal Society, United Kingdom; the Russian Foundation for Basic Research; the Ministerio de Ciencia e Innovación, and Programa Consolider-Ingenio 2010, Spain; the Slovak R&D Agency; the Academy of Finland; the Australian Research Council (ARC); and the EU community Marie Curie Fellowship Contract No. 302103.

-
- [1] E. Braaten, J. Lee, and S. Fleming, Associated production of ν and weak gauge bosons at the Tevatron, *Phys. Rev. D* **60**, 091501 (1999).
- [2] B. Gong, J.-P. Lansberg, C. Lorce, and J. Wang, Next-to-leading-order QCD corrections to the yields and polarisations of J/Ψ and Upsilon directly produced in association with a Z boson at the LHC, *J. High Energy Phys.* **03** (2013) 115.
- [3] P. Artoisenet, F. Maltoni, and T. Stelzer, Automatic generation of quarkonium amplitudes in NRQCD, *J. High Energy Phys.* **02** (2008) 102.
- [4] D. Acosta *et al.* (CDF Collaboration), Search for Associated Production of Υ and Vector Boson in $p\bar{p}$ Collisions at $\sqrt{s} = 1.8 \text{ TeV}$, *Phys. Rev. Lett.* **90**, 221803 (2003).
- [5] G. Aad *et al.* (ATLAS Collaboration), Measurement of the production cross section of prompt J/ψ mesons in association with a W^\pm boson in pp collisions at $\sqrt{s} = 7 \text{ TeV}$ with the ATLAS detector, *J. High Energy Phys.* **04** (2014) 172.
- [6] G. Aad *et al.* (ATLAS Collaboration), Measurement of the production cross section of prompt J/ψ mesons in association with a W^\pm boson in pp collisions at $\sqrt{s} = 7 \text{ TeV}$ with the ATLAS detector, Report No. CERN-PH-EP-2014-276.
- [7] F. Abe *et al.* (CDF Collaboration), The CDF detector: An overview, *Nucl. Instrum. Methods Phys. Res., Sect. A* **271**, 387 (1988); D. E. Amidei *et al.* (CDF Collaboration), The silicon vertex detector of the collider detector at Fermilab, *Nucl. Instrum. Methods Phys. Res., Sect. A* **350**, 73 (1994); F. Abe *et al.* (CDF Collaboration), Measurement of the W boson mass, *Phys. Rev. D* **52**, 4784 (1995); S. Cihangir, G. Gillespie, H. Gonzalez, S. Gonzalez, C. Grimm, M. Guerra, T. Hawke, M. Hrycyk *et al.*, SVX': The new CDF silicon vertex detector, *Nucl. Instrum. Methods Phys. Res., Sect. A* **360**, 137 (1995); R. Blair *et al.* (CDF Collaboration), The CDF-II detector: Technical design report, Report No. FER-MILAB-DESIGN-1996-01.
- [8] D. Acosta *et al.* (CDF Collaboration), The CDF Cherenkov luminosity monitor, *Nucl. Instrum. Methods Phys. Res., Sect. A* **461**, 540 (2001).
- [9] J. Alwall, P. Demin, S. de Visscher, R. Frederix, M. Herquet, F. Maltoni, T. Plehn, D.L. Rainwater, and T. Stelzer, MadGraph/MadEvent v4: The new web generation, *J. High Energy Phys.* **09** (2007) 028.
- [10] E. Braaten, S. Fleming, and A.K. Leibovich, NRQCD analysis of bottomonium production at the Tevatron, *Phys. Rev. D* **63**, 094006 (2001).
- [11] R. Sharma and I. Vitev, High transverse momentum quarkonium production and dissociation in heavy ion collisions, *Phys. Rev. C* **87**, 044905 (2013).
- [12] T. Sjöstrand, S. Mrenna, and P.Z. Skands, PYTHIA 6.4 physics and manual, *J. High Energy Phys.* **05** (2006) 026.
- [13] R. Brun, F. Carminati, and S. Giani, GEANT detector description and simulation tool, Report No. CERN-W5013.
- [14] E. Gerchtein and M. Paulini, *CDF detector simulation framework and performance*, eConf C0303241, TUMT005 (2003).
- [15] A. Abulencia *et al.* (CDF Collaboration), Measurements of inclusive W and Z cross sections in p anti- p collisions at $\sqrt{s} = 1.96\text{-TeV}$, *J. Phys. G* **34**, 2457 (2007).
- [16] T. Aaltonen *et al.* (CDF Collaboration), Measurements of angular distributions of muons from Υ meson decays in $p\bar{p}$ collisions at $\sqrt{s} = 1.96 \text{ TeV}$, *Phys. Rev. D* **88**, 052012 (2013).
- [17] T. Aaltonen *et al.* (CDF Collaboration), Searches for the Higgs Boson Decaying to $W^+W^- \rightarrow \ell^+\nu\ell^-\bar{\nu}$ with the CDF II Detector, *Phys. Rev. Lett.* **108**, 151802 (2012).
- [18] J. Pumplin, D. R. Stump, J. Huston, H. L. Lai, P. M. Nadolsky, and W. K. Tung, New generation of parton distributions with uncertainties from global QCD analysis, *J. High Energy Phys.* **07** (2002) 012.
- [19] A. D. Martin, W. J. Stirling, R. S. Thorne, and G. Watt, Parton distributions for the LHC, *Eur. Phys. J. C* **63**, 189 (2009).
- [20] J. Beringer *et al.* (Particle Data Group), Review of particle physics (RPP), *Phys. Rev. D* **86**, 010001 (2012).
- [21] T. Aaltonen *et al.* (CDF Collaboration), Observation of single top quark production and measurement of $-\text{V}t\text{b}$ with CDF, *Phys. Rev. D* **82**, 112005 (2010).